The International Journal of Advanced Manufacturing Technology (2023) 125:2055–2064
https://doi.org/10.1007/s00170-023-10805-7

ORIGINAL ARTICLE

Room temperature enhancement of flexural strength in silicon carbide green body via the addition of cellulose nanofiber

Teruyoshi Kanno[1] · **Hiroki Kurita**[1] · **Fumio Narita**[1]

Received: 29 June 2022 / Accepted: 1 January 2023 / Published online: 16 January 2023

Abstract
Silicon carbide (SiC) green bodies fabricated using robocasting were strengthened by incorporating cellulose nanofiber (CNF) into a SiC slurry and just drying at room temperature. The measured flexural strength of a SiC green body modified via the CNF with a liquid phase weight ratio (water-to-CNF slurry) of 80:20 was 813 ± 37 kPa, 1.5 times larger than the strength of an unmodified green body. The strength was improved due to the increased number of hydrogen-bonding sites between the raw particles and CNF. After annealing at 250 °C, the lowering of the flexural strength indicated the occurrence of the bonding sites via water that was trapped on the CNF. The addition of CNF increased the viscosity and yield stress of the SiC slurry, which remained in the Bingham pseudoplastic behavior regardless of the CNF used. Moreover, this addition showed no effect on the relative densities, microstructures, and crystalline phases of the sintered SiC body. Therefore, the addition of CNF to the SiC slurry aided in handling the green body during processing and showed no detrimental effects on robocasting.

Keywords Additive manufacturing · SiC · Green body strength · Cellulose nanofiber

1 Introduction

Silicon carbide (SiC) is a conventional structural ceramic material due to its low density, high mechanical properties, and thermal stability, and it has been applied as a structural material in aerospace and nuclear fields. SiC components have been mainly fabricated by chemical vapor infiltration, polymer impregnation and pyrolysis, liquid silicon infiltration, solid-state sintering, and advanced hot pressing (e.g., spark plasma sintering and nano-infiltration and transient eutectic-phase (NITE) process) [1–6]. Significantly, the NITE process has attracted much attention as a suitable fabrication process to obtain fully dense SiC products. However, it is difficult to fabricate SiC with complex shapes due to the mechanical pressure applied to the product during the process, and subtractive manufacturing of SiC is also difficult due to its hardness.

In recent years, additive manufacturing (AM) has been the new fabrication process to obtain complex-shaped materials [7–12]. In this process, the ceramic slurry is automatically accumulated layer-by-layer, and a fabricated green body is debinded and densified by heat treatment. AM has been considered to fabricate SiC components with complex geometries, and combinations with three-dimensional modeling and sintering process without pressure have been studied. A fully crystalline SiC with a relative density of 92% has been fabricated by binder jet printing and chemical vapor infiltration [13]. SiC has been fabricated by a ultraviolet (UV) irradiation of a photocurable resin containing a ceramic precursor polymer, followed by pyrolysis and sintering [14].

Robocasting (also known as extrusion free-forming or direct ink writing), one of ceramic AM technologies, fabricates a green body by discharging slurry with specific rheological properties from a three-dimensionally controlled syringe. This method is inexpensive because no special equipment (e.g., UV or laser light) is required. SiC fabrication using robocasting has been combined with solid-state sintering using alumina (Al_2O_3) and yttria (Y_2O_3) as sintering additives or spark plasma sintering [15, 16].

In the robocasting method, the rheological properties of the slurry, such as suitable viscosity for discharge and Bingham pseudoplastic characteristics, which show shear-thinning viscosity and initial yield stress, are essential. Shear-thinning facilitates the discharge of the slurry from a nozzle because the

✉ Fumio Narita
narita@material.tohoku.ac.jp

[1] Department of Frontier Sciences for Advanced Environment, Graduate School of Environment Studies, Tohoku University, Sendai, Japan

viscosity decreases at high shear rates during extrusion. The initial yield stress, a critical point where the slurry with elastic behavior starts to flow, prevents deformation after discharge and lamination. Their acceptable values are determined by the performance of robocasting system used (e.g., if the yield stress of a slurry is too high, the slurry requires high load to start to flow). In addition, high viscosity in static conditions prevents the slurry from dripping and maintains a printed shape after discharge [17]. However, the strength of the dried green body fabricated using robocasting is an issue for its handleability and complex shape fabrication since it is more fragile and has lower strength than its sintered body.

The enhancement of green body strength has been attempted in some studies. Previous studies found that the strength of green bodies can be improved by presintering or adding cellulose nanocrystals (CNs) to a ceramic precursor gel and solidifying in powder compacting [18] or gel casting [19]. However, the compact body has a simple geometry, and a mold protects the casted gel in these studies; thus, these green bodies seem to have higher damage tolerance against any shocks during the fabrication processes than the green body with complex shapes fabricated using robocasting. Therefore, improving the strength of the robocasted green bodies directly and readily is desirable.

Research has focused on cellulose nanofiber (CNF) as a reinforcement of green bodies due to its high strength and chain structure [20, 21]. The low CNF addition can strengthen a matrix [22, 23]. In Ref. [22, 23], epoxy resin was strengthened by the CNF addition of less than 0.5 vol.%. It was concluded that the strengthening mechanism could occur by a chemical interaction between epoxy resin and CNF. An aqueous slurry containing CNF has thixotropic and shear-thinning behavior, and a rigid cellulose sheet remained after drying [24]. Therefore, CNF slurry is expected to strengthen green bodies by simple drying without changing the slurry rheology.

This study clarified the effects of CNF slurry on robocasting for SiC. SiC slurry rheology containing the CNF slurry was measured. The CNF effect on the green body strength was discussed by comparing the flexural strength of the green bodies made from slurries with the different concentrations of CNF and the quality of the sintered bodies. In addition, a strengthening mechanism of the green body was verified experimentally by comparing the flexural strength of the green bodies after annealing at temperatures that caused a change in the morphology of the CNF.

2 Experimental procedure

2.1 Materials

α-SiC powder (D_{50} = 0.61 μm; GMF 15H2, Pacific Rundum Co., Ltd., Japan) was prepared as a starting material. Boron carbide (B_4C) powder (particle size 1–7 μm, F-1200, ESK Ceramics GmbH & Co. KG, Germany) and carbon powder (particle size 29 nm; Niteron #200, Nippon Steel Carbon Co., Ltd., Japan) were prepared as sintering additives. The weight fractions of B_4C and C were controlled at 0.5 and 2.5 wt.%. A commercial polycarboxylic acid aqueous solution (Celuna D-735, Chu-kyo Yushi Co., Ltd., Japan) was used as a dispersant, and its concentration was controlled at 0.5 mg/m^2 for the SiC powder that has a specific area of 16.4 m^2/g. As reinforcement, mechanically homogenized CNF aqueous slurry of 2 wt.% (BiNFi-s IMa-10002, Sugino Machine Ltd., Japan) was used.

2.2 Slurry preparation

Although there are many parameters that affect the fabricated green body strength, we focus on the amount of CNF addition. Aqueous dispersion media were prepared by mixing the ion-exchanged water, CNF slurry, and dispersant for 30 s using a planetary mixer (a revolution speed of 2000 rpm, revolution-to-rotation ratio = 5:2, AR-50, THINKY Co., Japan). In this process, its liquid phase weight ratio (water-to-CNF slurry) was controlled at 100:0, 90:10, and 80:20, and each slurry was denoted by its weight ratio. B_4C and C were added to the media and stirred for 30 s. Then, the slurry was further stirred with SiC for 1 min and defoamed for 30 s at a revolution speed of 2200 rpm without rotation. Finally, SiC slurry with SiC solid loading of 40 vol.% was obtained.

2.3 Robocasting and sintering

The robocasting system was composed of an air pulse dispenser (ML-808GX, Musashi Engineering, Inc., Japan) and a three-axis automatic robot with a 30 mL syringe and a 1.6 mm diameter conical nozzle (SHOTmini 200ΩX, Musashi Engineering, Inc., Japan) as shown in Fig. 1. Modeling shapes were designed to a length of 40 mm × 3 rows in the *y*-direction with a width span of 1.5 mm × 3 layers in the *z*-direction with a layer span of 2.0 mm (see Fig. 2) for a flexural test and to a length of 10 mm × width of 10 mm, a width span of 2.0 mm × 2 layers in the *z*-direction, and a layer span of 2.0 mm for a sintering test. The prepared slurry was discharged to a wax-coated aluminum stage with a printing speed of 30 mm/s, and a discharge flow rate was fixed at 0.17 cm^3/s by adjusting the pressure to a range of 70–170 kPa.

The green body can fracture by any shocks during transportation to the furnace. If the product is strengthened on the stage after 3D fabrication and drying, the fracture can be avoided. So the discharged slurries were dried on the stage at room temperature (RT) for a day. The role of drying was to

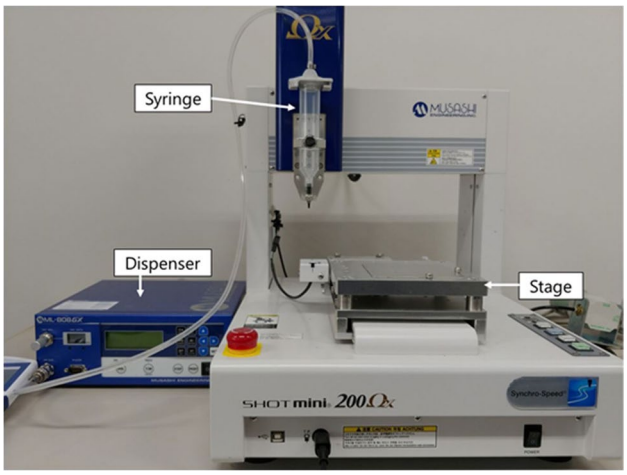

Fig. 1 Modeling system for robocasting

remove water and it was removed almost completely (above 90 wt.%).

For fabrication of sintered bodies, the green bodies were debinded at 400 °C for 2 h using a heating rate of 50 °C/min under vacuum, followed by sintering at 2000 °C for 1 h using a heating rate of 50 °C/min in argon gas. These processes were conducted without mechanical pressure, and no cracks were observed after the heat treatments.

2.4 Characterization

To investigate whether the slurry exhibited Bingham pseudoplastic behavior, rheological measurement was carried out using a rotational rheometer (HAAKE RheoStress 6000, Thermo Fisher Scientific, USA) with a 35-mm diameter parallel plate and 0.5-mm gap at room temperature. The CNF slurry, SiC slurry without CNF (100:0 slurry), and SiC slurry with CNF (80:20 slurry) were prepared as test specimens. The slurries were preshared at a shear rate of 1 s^{-1} for 1 min, followed by a resting state for 20 min. Subsequently, the shear rate was controlled at 0.01–100 s^{-1}.

Thermogravimetric analysis (TGA) was conducted using a thermal analyzer (SDT Q600, TA Instruments, USA) at 50–600 °C using a heating rate of 10 °C/min under Ar flow for the determination of the debinding condition and CNF morphology. The 100:0 and 80:20 slurries were served as powder crushed in a mortar after drying for a day. Meanwhile, a dried CNF sample was obtained by drying the raw CNF slurry at room temperature.

This study adopted flexural strength obtained from a three-point flexural test to characterize green body strength after drying at room temperature for 2 days. This test was performed using a universal testing machine (AG-Xplus, Shimadzu Co., Japan) under a 30-mm span and a 0.5-mm/min crosshead speed. Tested green bodies were fabricated with the 100:0, 90:10, and 80:20 slurries. They were formed and polished with abrasive paper to the size of about 40 mm × 6 mm × 5 mm before the test. Their microstructures and CNF were observed using a field emission scanning electron microscope (FE-SEM, SU-70, Hitachi High-Tech Corporation, Japan) to determine CNF strengthening mechanism.

For further discussion, the three-point flexural test of green bodies annealed at 250 and 500 °C was also performed at room temperature. Bound water trapped on CNF desorbed from 250 °C. CNF started to pyrolyze from 300 °C. To identify the factors that influenced the green body strength, we annealed the green bodies at 250 °C, where the bound water desorbed but only the CNF remained, and at 500 °C, where the CNF themselves had been almost completely pyrolyzed. These temperatures for annealing were determined based on a result of TGA described in Sect. 3.2. The crashed green bodies annealed at the temperatures were examined by Fourier transform infrared spectroscopy (FT-IR, FT/IR-6300 and IRT-7000, JASCO Corporation, Japan).

The effect of CNF on the sintered bodies was evaluated using the 100:0 and 80:20 sintered bodies for the following three perspectives: microstructure, crystal composition, and relative density. Microstructures were observed using FE-SEM. The crystal composition was analyzed by X-ray diffraction (XRD, Ultima IV, Rigaku Corporation, Japan). The bulk density of rod- and square-shaped samples was measured using the Archimedes method. Subsequently, the relative density was calculated using the bulk density and a theoretical density of 3.18 g/cm^3 defined from the theoretical densities of SiC, C, and B_4C.

3 Results and discussion

3.1 Rheological properties

Figure 3 shows the rheological properties, namely, shear rate $\dot{\gamma}$ shear stress τ, and shear rate viscosity η relationship, of the CNF, 100:0 slurry, and 80:20 slurry. All slurries had Bingham pseudoplastic behavior, i.e., yield stress and shear thinning. The yield stress can be estimated using the Herschel–Bulkley model (Eq. 1) [25]

$$\tau = \tau_y + k\dot{\gamma}^n \quad (1)$$

where τ_y is the yield stress, and k and n are constants. The estimated yield stresses of the CNF, 100:0 slurry, and 80:20 slurry were 36.5, 7.59, and 49.5 Pa, respectively, by fitting the equation in the τ–$\dot{\gamma}$ curve except for unstable low shear rate ($\dot{\gamma} < 1$) in 100:0 and 80:20 slurries (Fig. 3a). Coefficient of determination R^2 was calculated based on the experimental value and the theoretical value using the fitting parameters. R^2 of the CNF, 100:0, and 80:20 slurries were 0.987, 0.995, and 0.903, respectively.

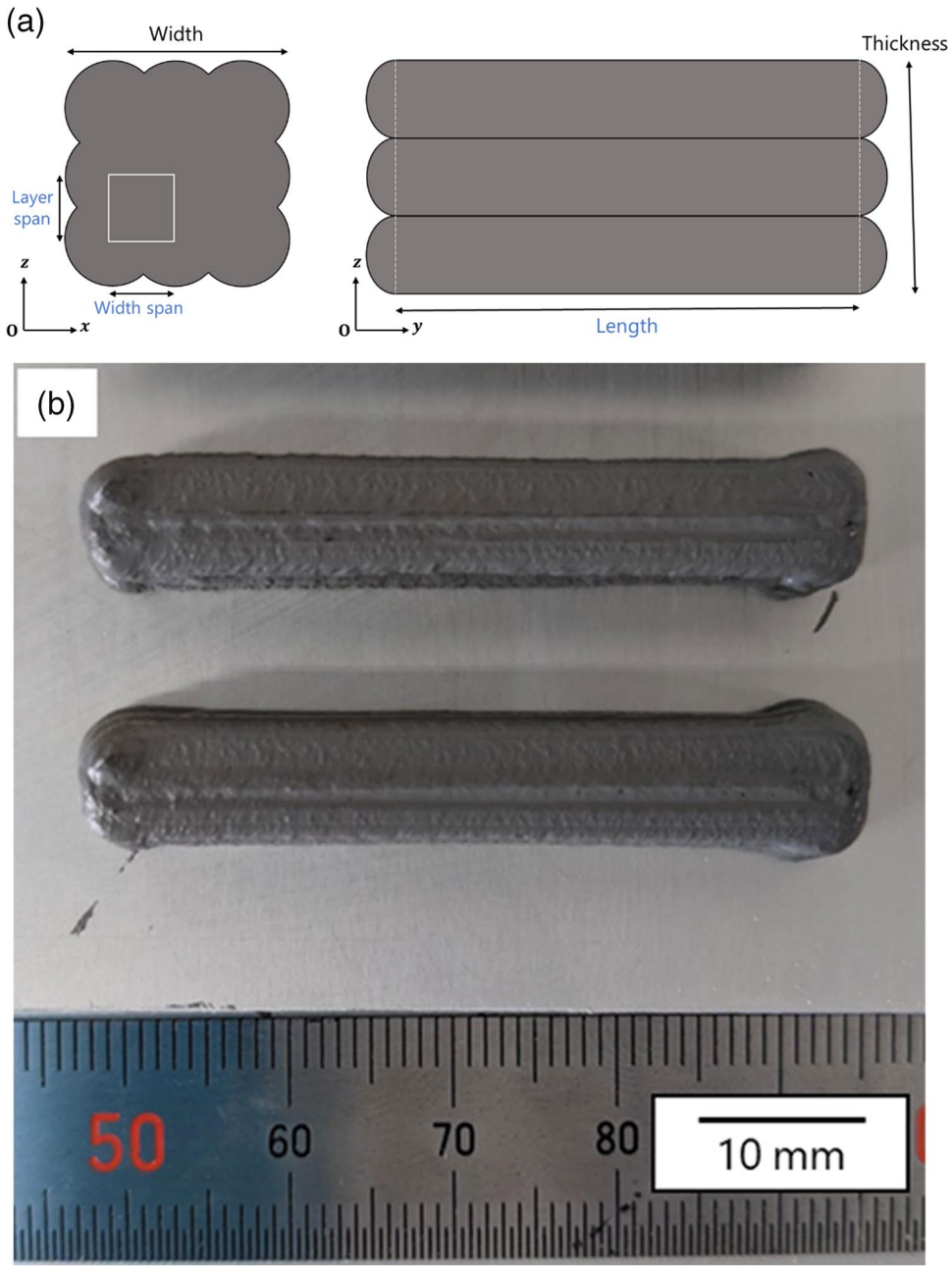

Fig. 2 **a** Schematic of the relationship between modeling parameters and actual sizes: variable parameters are written in blue, **b** robocasted slurry for the flexural test

The unstable region might appear due to slippage on the plate, flow heterogeneity, or a transient response during the transition from an elastic rest state to a fluid state during start-up [17, 26]. The yield stress of the SiC slurry increased with CNF slurry addition, which indicated that the CNF addition improved the shape retention ability of the slurry after robocasting. However, the capacity of CNF was dependent on the modeling conditions, particularly discharge pressure. The more CNF was added, the more discharge pressure was required. Therefore, this study limited the water-to-CNF slurry ratio in the medium to 80:20.

3.2 Thermogravimetric analysis

Figure 4a shows a TGA profile of the dried CNF slurry. The CNF showed a typical TG curve of cellulose: bound water on CNF dissipated around 250 °C, and the CNF pyrolyzed above 300 °C [27, 28]. Figure 4b shows the TGA profiles of the 100:0 and 80:20 slurries. The weight-loss curve of the 80:20 slurry was different from that of the 100:0 slurry and can be divided into three temperature regions (Fig. 4b). In region 1 (50–250 °C), most of the water from the medium evaporated as free water. However, some water remained

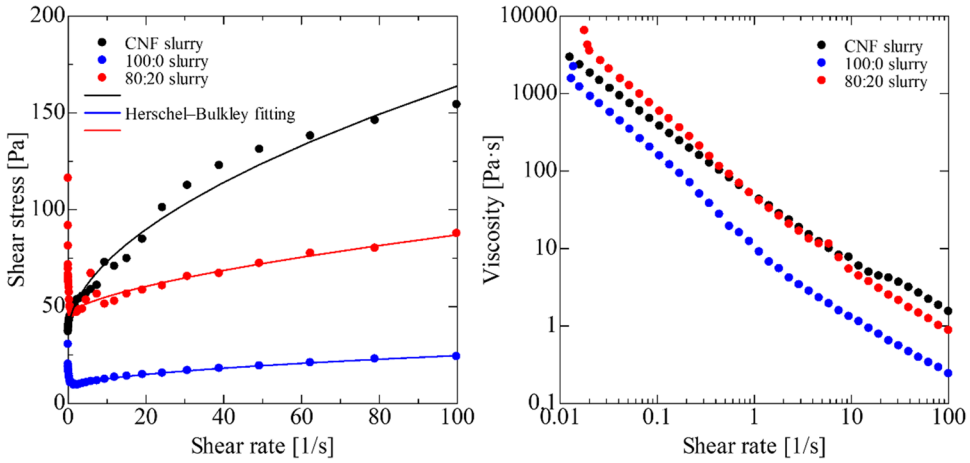

Fig. 3 Rheological properties of the fabricated slurries compared to raw CNF slurry. **a** τ–$\dot{\gamma}$ and **b** η–$\dot{\gamma}$ curves

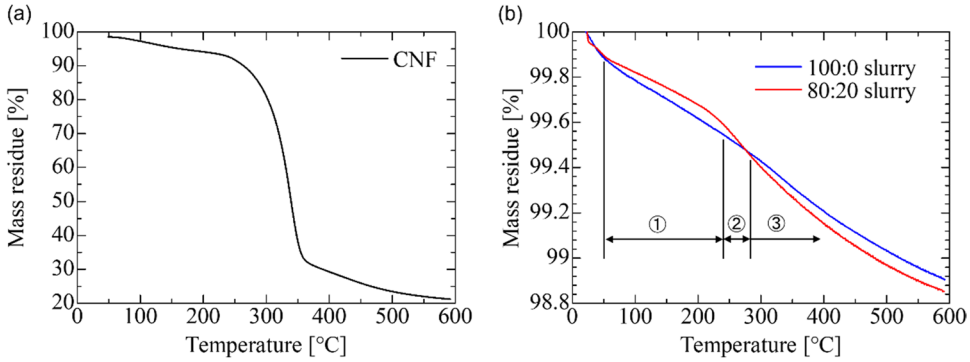

Fig. 4 Weight-reduction curve of **a** the dried CNF sheet and **b** the fabricated slurries obtained using thermogravimetric analysis

as the bound water on CNF with numerous hydroxyl groups. Consequently, the weight loss of the 80:20 slurry was lower than that of the 100:0 slurry. In region 2 (around 250 °C), only the 80:20 slurry showed significant weight loss, indicating that the bound water was released from CNF. In region 3 (300 °C–), the pyrolysis of CNF progressed, and the percent mass residue fell below a value corresponding to the weight fraction of CNF (approximately 0.175 wt.%). Meanwhile, the weight of the 100:0 slurry decreased over the entire region because the dispersant vaporized and pyrolyzed.

3.3 Green body strength

Figure 5 shows the flexural strength of the green bodies with different CNF concentrations. The flexural strength of the green body fabricated with the 80:20 slurry (813 ± 37 kPa) was 1.5 times larger than that of the green body fabricated with the 100:0 slurry (539 ± 68 kPa). The flexural strength of the green body fabricated via the 90:10 slurry (634 ± 50 kPa) was between those of the 100:0 and 80:20 green bodies. After the flexural testing, flat surface was shown in the green bodies. The microstructures of the 100:0 and 80:20 green bodies are shown in Fig. 6. Slender CNFs (Fig. 6c) were observed in multiple locations in the 80:20 green body. The

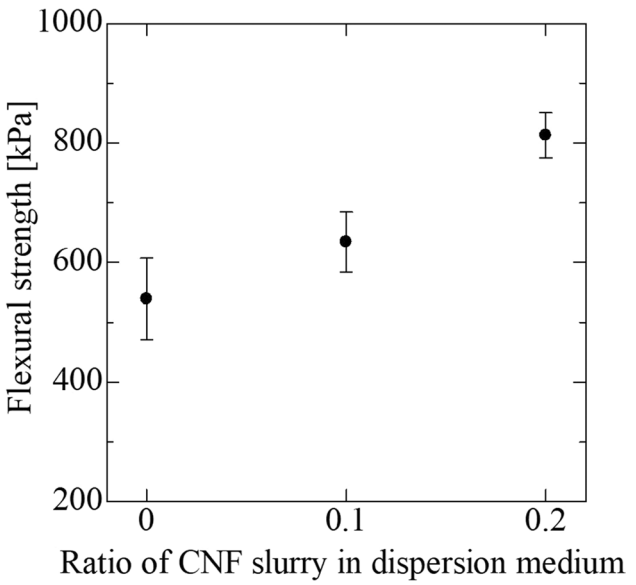

Fig. 5 Flexural strength of the dried green bodies with different CNF concentrations obtained by the three-point flexural test

microstructure of the 80:20 green body shows the adsorption between CNF and the raw particles and among the particles. This indicates that CNF causes an increase in the number of bound sites, which may improve flexural strength because the abundance of the bonding sites forms a dense network to support the structure and consumes the fracture energy when the crack propagates [29].

To determine the CNF strengthening mechanism, the flexural strength of the "brown" bodies, which were annealed at 250 °C to dissipate the bound water and at 500 °C to pyrolyze CNF, was investigated as shown in Fig. 7a. The strength of the 80:20 brown body annealed at 250 °C decreased to the same level as that of the 100:0 green body, whereas the strength of the 100:0 green body remained unchanged after annealing at 250 °C. Therefore, the bound water on CNF contributed to enhancing the green body.

It is noted that the bound water and hydroxyl groups of CNF form a three-dimensional network derived from their hydrogen bonds in CNFs. They have enhanced the polymer-matrix composites containing CNF and CNF compressed dry bulk [30, 31]. On the other hand, SiC and carbon black are partially oxidized in water, and their surfaces have hydrogen-bonding sites, such as the silanol group [32–34]. The results suggest that the green body was strengthened by increased bonding sites in the green body where the hydrogen bonding through the bound water was dominant (see Fig. 7b).

Using cellulose, previous studies enhanced strength by adding CNs and solidifying at 60–70 °C or by adding carboxymethyl cellulose (CMC) and solidifying at 50–70 °C to facilitate the crosslink condensation reaction between CMC and dispersant [19, 35]. While these studies conducted heat treatments, the present study achieved the enhancement by room temperature drying. Table 1 presents the comparison of the green body strength of SiC from this study with the ceramic materials from the literature [19, 35]. It is interesting to note that the use of CNF as a reinforcement has the same effect as other ceramic materials in improving strength even at room temperature.

The CNF strengthening mechanism through hydrogen bonding explains the increase in the green body strength without annealing. However, it does not apply to strength enhancement after annealing at 500 °C (see Fig. 7) because the bound water and CNF seem to dissipate based on the TGA result. The strength enhancement after annealing at 500 °C may be due to an increase in nonpolar groups on the SiC surface. The bound water is a hydrogen-bonding site released at 250 °C. Meanwhile, the polar groups remained on the surface of the raw particles. Therefore, the polar sites compete with the nonpolar sites, such as siloxane and native Si–C combination on the surface, thus limiting the effective bonding sites by decreasing the hydrogen-bonding sites. However, since desorption of the polar groups at 500 °C causes occupation of the nonpolar sites on the surface, van der Waals interaction becomes dominant, which increases the effective bonding sites to improve the strength again. This strength trend is consistent with the tensile test results for a powder bed with silica glass particles, as reported in a previous study [36]. The deviation trend in Figs. 5 and 7 was also consistent with that in its reference because the green body was a powder aggregate, similar to the powder

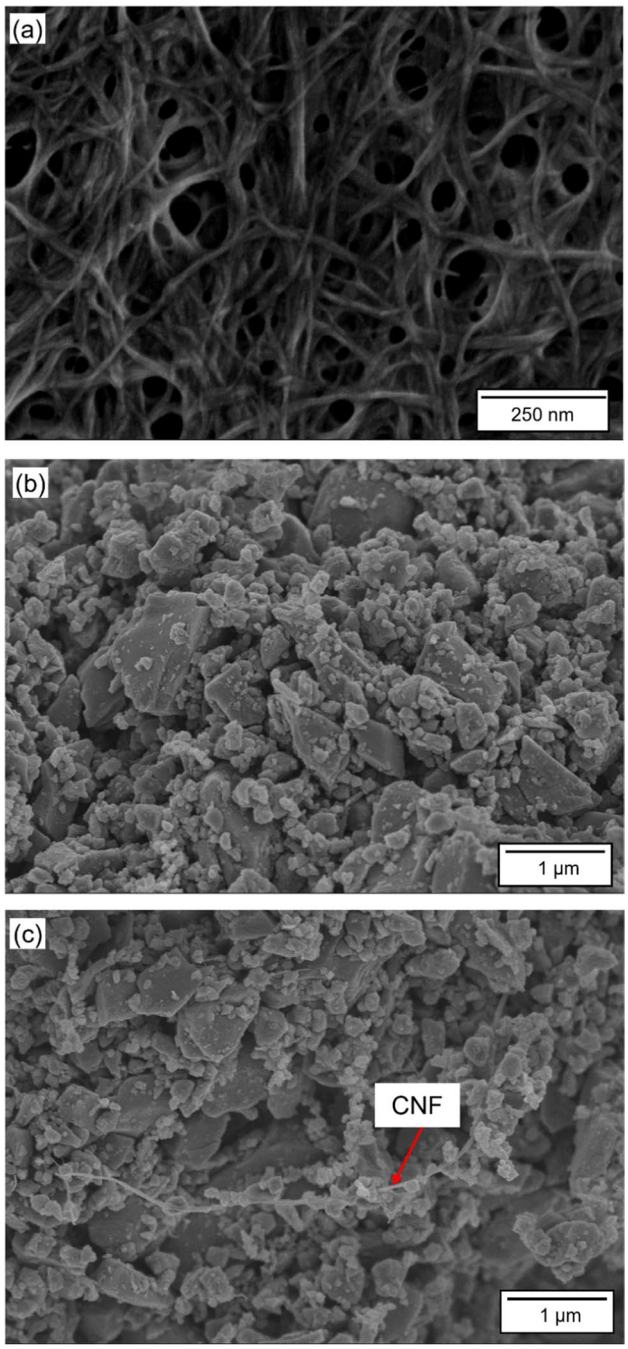

Fig. 6 SEM cross-sectional images of **a** the dried CNF slurry and the green bodies fabricated with the **b** 100:0 and **c** 80:20 slurries

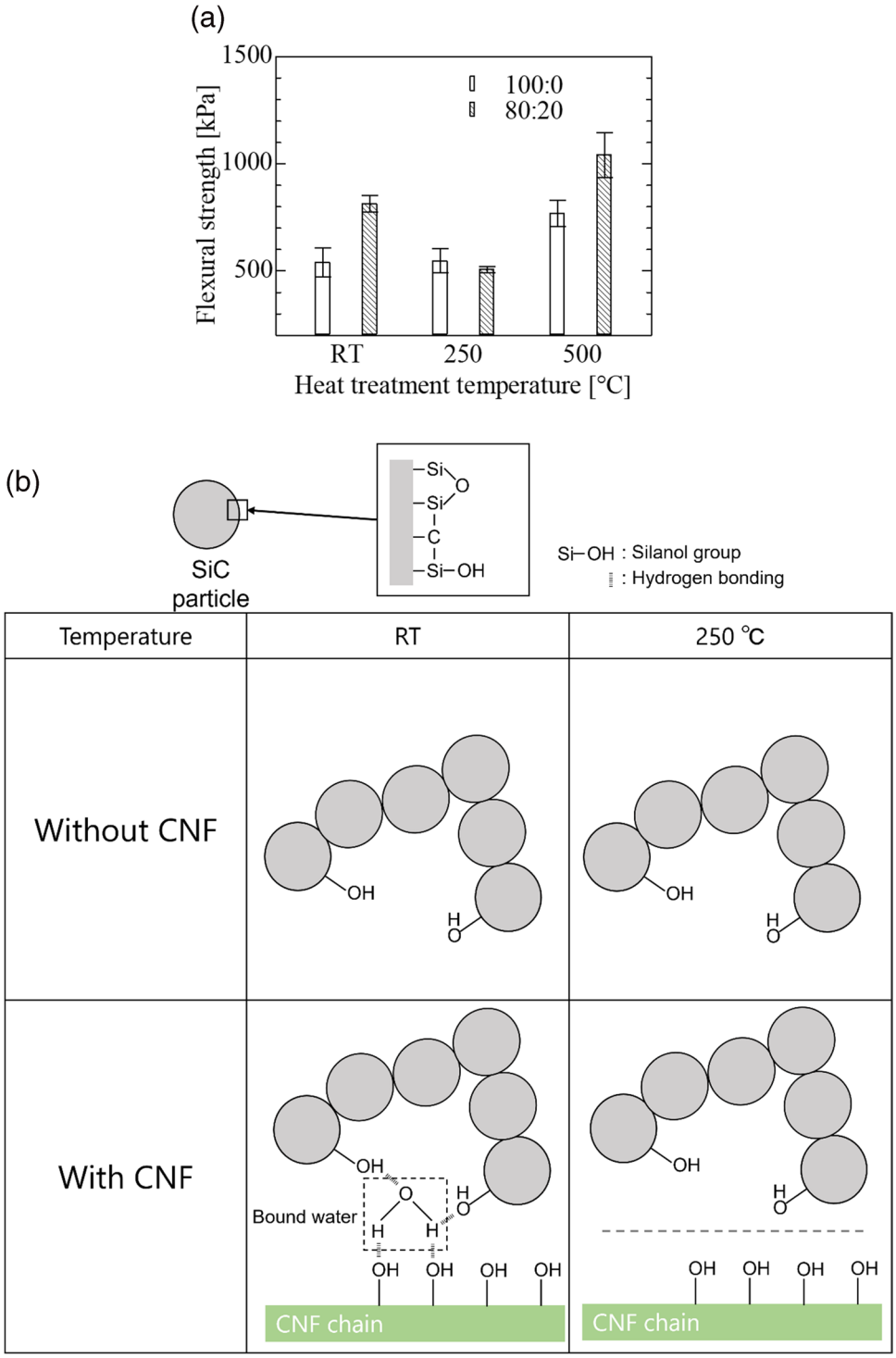

Fig. 7 **a** Flexural strength of the brown bodies after heat treatment at bound water desorption or CNF pyrolysis temperatures. **b** Schematic diagram of the bonding between the SiC particle and the SiC particle or the CNF in the green bodies at room temperature and 250 °C

bed. The difference in 500 °C between the 100:0 and 80:20 brown bodies should be investigated further.

We conducted IR measurement with attenuated total reflection for hydrogen-bonding characterization. However, the powder samples fabricated with crushed green bodies showed a similar profile regardless of CNF presence and heat treatment temperature (RT, 250 °C, 500 °C). That was because Si–C absorbance was too strong, and the CNF amount was too small. Hence, we performed the test using dried pure CNF slurry. The CNF showed a typical spectrum profile of cellulose. On the other hand, the intensity of the CNF heated at 250 °C was entirely lower than that without heat treatment. In addition, dehydration

Table 1 Green body strength of ceramics compared with other reported conditions

Drying temp. (°C)	Materials	Reinforcement	Strength (Pa)	Deformation	Fabrication method	Ref
25	SiC	–	539×10^3	Bending	Robocasting	This study
		CNF	813×10^3			
Dry: 60–70 Cure: 90	Al_2O_3 + PDMAA	–	15.3×10^6	Bending	Gel casting	[19]
		CNs	25.7×10^6			
50	SiC	CMC + PEI	1.21×10^6	Compressive	Gel casting	[35]
60			1.40×10^6			
70			1.90×10^6			

PDMAA poly(N,N-dimethylacrylamide), *PEI* polyethyleneimine

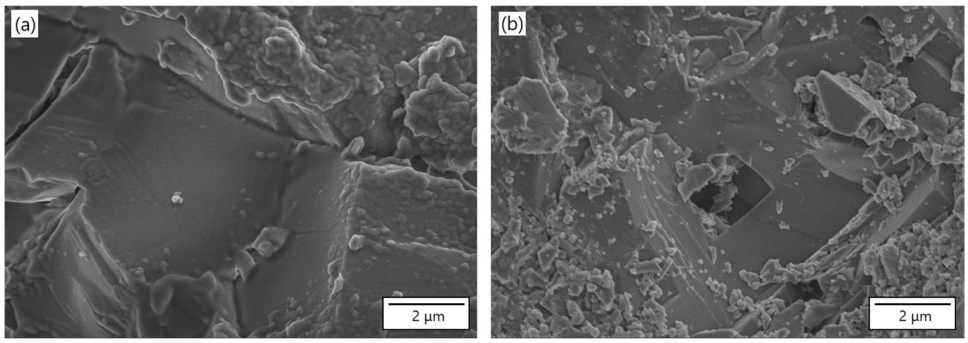

Fig. 8 SEM cross-sectional images of the sintered bodies fabricated with the **a** 100:0 and **b** 80:20 slurries

was observed by the lower intensity of the O–H band and the appearance of the C = C band.

3.4 Sintered body

The cross-sectional images of the sintered bodies fabricated with the 100:0 and 80:20 slurries are shown in Fig. 8. Regardless of the presence of CNF, both specimens exhibited brittle structures, and no clear difference was observed. The XRD patterns showed no difference in the crystalline phase between the 100:0 and 80:20 sintered bodies. The relative densities of the sintered bodies showed broad distribution, as shown in Fig. 9. This might be due to the separation of the raw materials in the slurry during defoaming, but there was almost no difference between the densities of the sintered bodies with CNF and those without CNF.

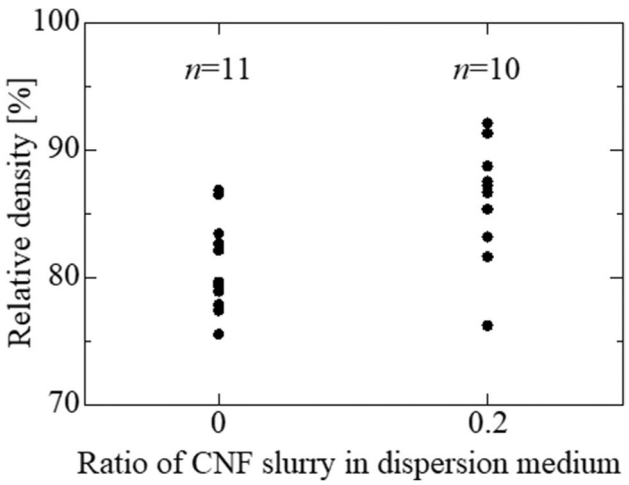

Fig. 9 Relative density distribution of the sintered bodies with different CNF concentrations (*n*: number of samples)

4 Conclusion

The SiC green body fabricated via robocasting was successfully strengthened by the commercial CNF slurry and simple drying without changing the qualitative rheological properties of the slurry and the microstructure of the sintered bodies. Moreover, the strength of the green bodies increased with CNF addition, which was caused by the increase in the number of hydrogen-bonding sites. This indicated that the handleability of the SiC green bodies could be improved by additives such as CNF, which provide hydrogen bonding sites at room temperature. This study presented the novelty in that the green bodies fabricated by robocasting were strengthened by drying at room temperature, which would be expected to expand the application of robocasting in terms of formability.

Acknowledgements The technical assistance provided by Katsuhiko Nobeta of Fuji Electric Industrial Co., Ltd. (Japan) on the sintering test is appreciated.

Author contribution Teruyoshi Kanno and Hiroki Kurita: research design. Teruyoshi Kanno: methodology, experiments, and writing the initial draft. Fumio Narita: supervisor and approval of the final manuscript.

Funding This work was supported by the Japanese Society for the Promotion of Science KAKENHI Grant Number JP 22J20100.

Data availability Not applicable.

Code availability Not applicable.

Declarations

Ethics approval Not applicable.

Consent to participate Not applicable.

Consent for publication Not applicable.

Conflict of interest The authors declare no competing interests.

References

1. Igawa N, Taguchi T, Snead LL, Katoh Y, Jitsukawa S, Kohyama A, McLaughlin JC (2002) Optimizing the fabrication process for superior mechanical properties in the FCVI SiC matrix/stoichiometric SiC fiber composite system. J Nucl Mater 307–311:1205–1209. https://doi.org/10.1016/S0022-3115(02)01060-7
2. Kotani M, Inoue T, Kohyama A, Okamura K, Katoh Y (2002) Consolidation of polymer-derived SiC matrix composites: processing and microstructure. Compos Sci Technol 62:2179–2188. https://doi.org/10.1016/S0266-3538(02)00151-3
3. Margiotta JC, Zhang D, Nagle DC, Feeser CE (2008) Formation of dense silicon carbide by liquid silicon infiltration of carbon with engineered structure. J Mater Res 23:1237–1248. https://doi.org/10.1557/JMR.2008.0167
4. Tanaka H, Hirosaki N, Nishimura T (2003) Sintering of silicon carbide powder containing metal boride. J Ceram Soc Japan 111:878–882. https://doi.org/10.2109/jcersj.111.878
5. Katoh Y, Dong SM, Kohyama A (2002) Thermo-mechanical properties and microstructure of silicon carbide composites fabricated by nano-infiltrated transient eutectoid process. Fusion Eng Des 61–62:723–731. https://doi.org/10.1016/S0920-3796(02)00180-1
6. Hayun S, Paris V, Mitrani R, Kalabukhov S, Dariel MP, Zaretsky E, Frage N (2012) Microstructure and mechanical properties of silicon carbide processed by Spark Plasma Sintering (SPS). Ceram Int 38:6335–6340. https://doi.org/10.1016/j.ceramint.2012.05.003
7. Rodrigues TA, Duarte VR, Tomás D, Avila JA, Escobar JD, Rossinyol E, Schell N, Santos TG, Oliveira JP (2020) In-situ strengthening of a high strength low alloy steel during wire and arc additive manufacturing (WAAM). Addit Manuf 34:101200. https://doi.org/10.1016/j.addma.2020.101200
8. Li S, Li JY, Jiang ZW, Cheng Y, Li YZ, Tang S, Leng JZ, Chen HX, Zou Y, Zhao YH, Oliveira JP, Zhang Y, Wang KH (2022) Controlling the columnar-to-equiaxed transition during directed energy deposition of Inconel 625. Addit Manuf 57:102958. https://doi.org/10.1016/j.addma.2022.102958
9. Rodrigues TA, Bairrão N, Farias FWC, Shamsolhodaei A, Shen J, Zhou N, Maawad E, Schell N, Santos TG, Oliveira JP (2022) Steel-copper functionally graded material produced by twin-wire and arc additive manufacturing (T-WAAM). Mater Des 213:110270. https://doi.org/10.1016/j.matdes.2021.110270
10. Nakajima K, Leparoux M, Kurita H, Lanfant B, Cui D, Watanabe M, Sato T, Narita F (2022) Additive manufacturing of magnetostrictive Fe–Co alloys. Materials (Basel) 15:1–12. https://doi.org/10.3390/ma15030709
11. Kurita H, Lohmuller P, Laheurte P, Nakajima K, Narita F (2022) Additive manufacturing and energy-harvesting performance of honeycomb-structured magnetostrictive Fe_{52}–Co_{48} alloys. Addit Manuf 54:102741. https://doi.org/10.1016/j.addma.2022.102741
12. Kurita H, Bernard C, Lavrovsky A, Narita F (2021) Tensile properties of mechanically-defibrated cellulose nanofiber-reinforced polylactic acid matrix composites fabricated by fused deposition modeling. Trans Nanjing Univ Aeronaut Astronaut 38:68–74. https://doi.org/10.16356/j.1005-1120.2021.01.006
13. Terrani K, Jolly B, Trammell M (2020) 3D printing of high-purity silicon carbide. J Am Ceram Soc 103:1575–1581. https://doi.org/10.1111/jace.16888
14. de Hazan Y, Penner D (2017) SiC and SiOC ceramic articles produced by stereolithography of acrylate modified polycarbosilane systems. J Eur Ceram Soc 37:5205–5212. https://doi.org/10.1016/j.jeurceramsoc.2017.03.021
15. Feilden E, Blanca EGT, Giuliani F, Saiz E, Vandeperre L (2016) Robocasting of structural ceramic parts with hydrogel inks. J Eur Ceram Soc 36:2525–2533. https://doi.org/10.1016/j.jeurceramsoc.2016.03.001
16. Cai K, Román-Manso B, Smay JE, Zhou J, Osendi MI, Belmonte M, Miranzo P (2012) Geometrically complex silicon carbide structures fabricated by robocasting. J Am Ceram Soc 95:2660–2666. https://doi.org/10.1111/j.1551-2916.2012.05276.x
17. M'Barki A, Bocquet L, Stevenson A (2017) Linking rheology and printability for dense and strong ceramics by direct ink writing. Sci Rep 7:1–10. https://doi.org/10.1038/s41598-017-06115-0
18. Li JZ, Wu T, Yu ZY, Zhang L, Chen GQ, Guo DM (2012) Micro machining of pre-sintered ceramic green body. J Mater Process Technol 212:571–579. https://doi.org/10.1016/j.jmatprotec.2011.10.030
19. Deng T, Wang Y, Dufresne A, Lin N (2018) Simultaneous enhancement of elasticity and strength of Al_2O_3-based ceramics body from cellulose nanocrystals via gel-casting process. Carbohydr Polym 181:111–118. https://doi.org/10.1016/j.carbpol.2017.10.058
20. Wu C, Egawa S, Kanno T, Kurita H, Wang Z, Iida E, Narita F (2021) Nanocellulose reinforced silkworm silk fibers for application to biodegradable polymers. Mater Des 202:109537. https://doi.org/10.1016/j.matdes.2021.109537
21. Samir MASA, Alloin F, Paillet M, Dufresne A (2004) Tangling effect in fibrillated cellulose reinforced nanocomposites. Macromolecules 37:4313–4316. https://doi.org/10.1021/ma035939u

22. Xie Y, Kurita H, Ishigami R, Narita F (2020) Assessing the flexural properties of epoxy composites with extremely low addition of cellulose nanofiber content. Appl Sci 10:1159. https://doi.org/10.3390/app10031159
23. Kurita H, Ishigami R, Wu C, Narita F (2021) Mechanical properties of mechanically-defibrated cellulose nanofiber reinforced epoxy resin matrix composites. J Compos Mater 55:455–464. https://doi.org/10.1177/0021998320967430
24. Lasseuguette E, Roux D, Nishiyama Y (2008) Rheological properties of microfibrillar suspension of TEMPO-oxidized pulp. Cellulose 15:425–433. https://doi.org/10.1007/s10570-007-9184-2
25. Herschel WH, Bulkley R (1926) Konsistenzmessungen von Gummi-Benzollösungen. Kolloid-Zeitschrift 39:291–300. https://doi.org/10.1007/BF01432034
26. Mewis J, Wagner NJ (2009) Thixotropy. Adv Colloid Interface Sci 147–148:214–227. https://doi.org/10.1016/j.cis.2008.09.005
27. Mu C, Guo J, Li X, Lin W, Li D (2012) Preparation and properties of dialdehyde carboxymethyl cellulose crosslinked gelatin edible films. Food Hydrocoll 27:22–29. https://doi.org/10.1016/j.foodhyd.2011.09.005
28. Quiévy N, Jacquet N, Sclavons M, Deroanne C, Paquot M, Devaux J (2010) Influence of homogenization and drying on the thermal stability of microfibrillated cellulose. Polym Degrad Stab 95:306–314. https://doi.org/10.1016/j.polymdegradstab.2009.11.020
29. Gonçalves RM, Martinho A, Oliveira JP (2022) Evaluating the potential use of recycled glass fibers for the development of gypsum-based composites. Constr Build Mater 321:126320. https://doi.org/10.1016/j.conbuildmat.2022.126320
30. Dagnon KL, Shanmuganathan K, Weder C, Rowan SJ (2012) Water-triggered modulus changes of cellulose nanofiber nanocomposites with hydrophobic polymer matrices. Macromolecules 45:4707–4715. https://doi.org/10.1021/ma300463y
31. Han X, Ye Y, Lam F, Pu J, Jiang F (2019) Hydrogen-bonding-induced assembly of aligned cellulose nanofibers into ultrastrong and tough bulk materials. J Mater Chem A 7:27023–27031. https://doi.org/10.1039/c9ta11118b
32. Studebaker ML, Huffman EWD, Wolfe AC, Nabors LG (1956) Oxygen-containing groups on the surface of carbon black. Ind Eng Chem 48:162–166. https://doi.org/10.1021/ie50553a044
33. Hallum JV, Drushel HV (1958) The organic nature of carbon black surfaces. J Phys Chem 62:110–117. https://doi.org/10.1021/j150559a031
34. Nojiri M, Matsui S, Hasegawa H, Ono T, Fukuda Y, Tsukada M, Kamiya H (2001) Analysis of anionic polymer dispersant behavior in dense silicon nitride and carbide suspensions using an AFM. J Nanoparticle Res 3:237–244. https://doi.org/10.1023/A:1017901222977
35. Gan K, Gai Y, Wang Y, Cui J, Lu Y, Zhang X, Liu J, Xu J, Yang J (2020) Direct coagulation casting of silicon carbide suspension via polyelectrolyte dispersant crosslink reaction. Int J Appl Ceram Technol 17:274–284. https://doi.org/10.1111/ijac.13328
36. Kamiya H, Kimura A, Yokoyama T, Naito M, Jimbo G (2002) Development of a split-type tensile-strength tester and analysis of mechanism of increase of adhesion behavior of inorganic fine powder bed at high-temperature conditions. Powder Technol 127:239–245. https://doi.org/10.1016/S0032-5910(02)00117-1